Bioactive Materials 3 (2018) 80–86

Contents lists available at ScienceDirect

Bioactive Materials

journal homepage: http://www.keaipublishing.com/en/journals/bioactive-materials/

Recyclable magnetite-silver heterodimer nanocomposites with durable antibacterial performance

Chunyan Yong, Xiaoqin Chen, Qian Xiang, Qiang Li, Xiaodong Xing*

College of Chemical Engineering, Nanjing University of Science and Technology, Nanjing 210094, China

ARTICLE INFO

Article history:
Received 26 April 2017
Received in revised form
26 May 2017
Accepted 31 May 2017
Available online 7 June 2017

Keywords:
Heterodimeric nanostructure
Antibacterial
Chitosan coating
Silver nanoparticle
Recyclable

ABSTRACT

There is a significant need for magnetite-silver nanocomposites that exhibit durable and recyclable antimicrobial activity. In this study, magnetic iron oxide nanoparticles (Fe_3O_4 NPs) coated with ethylenediamine-modified chitosan/polyacrylic acid copolymeric layer (Fe_3O_4@ECS/PAA) were fabricated. Subsequently, directly deposited silver (Ag) NPs procedure was carried out to form the antibacterial heterodimers of Fe_3O_4@ECS/PAA-Ag NPs. The composition and morphology of the resultant nanostructures were confirmed by FT-IR, XRD, TEM and TGA. The overall length of the heterodimers was approximately 45 nm, in which the mean diameter of Fe_3O_4@ECS/PAA NPs reached up to 35 nm, and that of Ag NPs was around 15 nm. The mass fraction of silver NPs in the nanocomposites was about 63.1%. The obtained Fe_3O_4@ECS/PAA NPs exhibited good colloidal stability, and excellent response to additional magnetic field, making the NPs easy to recover after antibacterial tests. In particular, the Fe_3O_4@ECS/PAA-Ag NPs retained nearly 100% biocidal efficiency (10^6–10^7 CFU/mg nanoparticles) for both Gram-negative bacteria *E. coli* and Gram-positive bacteria *S. aureus* throughout ten cycles without washing with any solvents or water, exhibiting potent and durable antibacterial activity.

1. Introduction

Silver nanoparticles (Ag NPs) have been extensively used over the past decade in various applications including catalysts, metal electrodes, biotechnology and bioengineering, medicine, and water treatment due to their unique electronic, optical, and catalytic properties [1–4]. Furthermore, they have also attracted considerable attention because of their excellent antibacterial property [5–7]. Currently, Ag NPs or their composites have been employed as effective antibacterial agents in a diverse range of consumer products. It is reported that the antibacterial properties of silver are closely related to the size of nanoparticles [8]. Unfortunately, Ag NPs synthesized using conventional methods aggregate easily, which greatly decreases their antibacterial activity [9]. To solve this problem, Ag NPs have been loaded onto suitable matrix, such as silicon dioxide [10,11], cellulose fiber [12,13], carbon nanotube [14,15,18] and graphene oxide [16–18].

Thanks of the large surface area and superparamagnetism, Fe_3O_4 nanoparticles (Fe_3O_4 NPs) have found a lot of applications in various fields [19–21]. Combining Fe_3O_4 NPs and Ag NPs can not only prevent the coalescence of Ag NPs, but also achieve recycling of nanosized silver to avoid contamination of surroundings. Bhupendra Chudasama et al. [22] synthesized Fe_3O_4-Ag core-shell nanostructures and studied their antimicrobial activity and molecular mechanism. In their work, hydrophobic Fe_3O_4-Ag nanostructures realized phase transfer via ligand exchange, improving the dispersibility in water. Xia et al. [9] synthesized Fe_3O_4@C@Ag nanocomposites with a mean diameter of 250 nm. The intermediate carbon layer protected magnetic core and improved the antibacterial activity of the Ag NPs. Compared to the Fe_3O_4 NPs, the decrease in the saturation magnetization for as-prepared samples can be attributed not only to the decreased content of the magnetic core, but also the Ag shell and the intermediate carbon layer. Tamim Mosaiab et al. [23] coated Fe_3O_4 NPs with poly (vinyl pyrrolidone) conjugated catechol (PVP-CCDP). Afterwards, silver nanoparticles were deposited onto PVP-CCDP coated iron oxide NPs by using remain catechol. The as-made nanoparticles could be removed easily through a magnet after antibacterial test and make it repeatable use. After five repeated uses, the antibacterial activity was declined by 20%.

* Corresponding author.
E-mail address: xingxiaodong07@njust.edu.cn (X. Xing).
Peer review under responsibility of KeAi Communications Co., Ltd.

http://dx.doi.org/10.1016/j.bioactmat.2017.05.008

The magnetic nanocomposites mentioned above possess Fe_3O_4@Ag core/shell structures. Gu et al. [24] described a methodology to form Fe_3O_4-Ag heterodimers based on the reactions on the colloidosome of organic solvent/water. The resultant heterodimeric nanostructures are composed of two distinct particles bound as a single entity and possess two different applied surfaces. The dual nature of heterodimeric nanostructures confers upon them fascinating properties [25,26]. To the best of our knowledge, using magnetic heterodimeric NPs as antibacterial agents has not been reported yet.

Chitosan (CS), which is produced by deacetylation of chitin, is a natural, biodegradable and biocompatible polysaccharide with high content of amino ($-NH_2$) groups [27–29]. Moreover, it exhibits "contact-killing" antibacterial activity, which functions similarly to general polycation compounds [30,31]. In this study, we fabricated recyclable antibacterial heterodimer nanocomposites like snowmen, which were composed of magnetic core coated with ethylenediamine-modified chitosan/polyacrylic acid (Fe_3O_4@ECS/PAA) NPs and Ag NPs. Successful preparation was evidenced by different techniques like Fourier Transform Infrared Spectra (FT-IR), Transmission Electron Microscope (TEM), X-Ray Diffraction (XRD), and Thermogravimetric Analysis (TGA). We also investigated the biocidal activity and magnetic recyclable property of as-prepared samples. The resultant heterodimeric nanoparticles exhibited powerful and long term antimicrobial activity. After ten cycles of antibacterial trials, the biocidal efficiency still remained nearly 100% for model microbes *E. coli* and *S. aureus*.

2. Experimental

2.1. Materials

Ferric chloride hexahydrate ($FeCl_3 \cdot 6H_2O$, ≥98%), ferrous chloride tetrahydrate ($FeCl_2 \cdot 4H_2O$, ≥99%), ammonium hydroxide (25–28%), sodium citrate (≥99%), acrylic acid (purified by distilling) and isoprophl alcohol (99.7%) were purchased from Chengdu Kelong Chemical Reagent Co. Ltd. (China). Chitosan (degree of deactylation 80–95%, Mw ~20,000) and poly (vinyl pyrrolidone) (PVP, Mw ~40,000) was obtained from Sinopharm. Chemical Reagent Co., Ltd. (China). Ammonium persulphate ($(NH_4)_2S_2O_8$, ≥98%) was purchased from United Initiators Co., Ltd. (China). Silver nitrate ($AgNO_3$, AR) was available from Shanghai Aladdin Chemistry Co. Ltd. (China).

2.2. Preparation of Fe_3O_4 nanoparticles

Fe_3O_4 NPs were prepared through an improved chemical coprecipitation method [32,33]. Briefly, $FeCl_2 \cdot 4H_2O$ (0.773 g) and $FeCl_3 \cdot 6H_2O$ (2.10 g) were dissolved in 160 mL of deionized water with 1:2 M ratio. Then, NH_3 aqueous solution (25 wt%) was added dropwise under vigorous mechanical stirring, and the final pH was maintained at about 10. Afterwards, the mixture was promptly heated to 80 °C and held for 30 min. After cooling to room temperature, the Fe_3O_4 NPs were separated by magnetic separation and washed with deionized water for three times.

2.3. Preparation of Fe_3O_4@ECS/PAA nanoparticles

To deposit polymer coatings efficiently, Fe_3O_4 NPs were modified with sodium citrate [34]. Briefly, Fe_3O_4 nanoparticles (107 mg) were dispersed in 40 mL of distilled water by sonication for 10 min and 40 mL sodium citrate (108 mg) aqueous solution were added. The contents was stirred for 2 h at 40 °C. Then, water-based magnetic fluid was obtained. Subsequently, the CS (1.0 g) was dissolved in 100 mL acrylic acid (0.60 g) water solution, and then magnetic fluid was added simultaneously. After N_2 bubbling for 30 min, approximately 30 mg of $(NH_4)_2S_2O_8$ as initiator was loaded in and polymerized at 80 °C for 8 h. The resulted Fe_3O_4@CS/PAA NPs were recovered by placing on a permanent magnet and washed with deionized water for three times. In order to further improve the hydrophilia and adsorption capacity of nanocomposites, Fe_3O_4@CS/PAA NPs were modified with ethylenediamine [35]. The Fe_3O_4@CS/PAA NPs (181 mg) were suspended in 30 mL isopropyl alcohol, to which 2 mL epichlorohydrine (25 mmol) dissolved in 40 mL acetone/water mixture (1:1 v/v) was added. The mixture was stirred for 24 h at 60 °C. The solid was separated by a permanent magnet and washed several times with water and ethanol. The solid obtained were suspended in 50 mL ethanol/water mixture (1:1 v/v), then ethylenediamine (2 mL) was added. The contents were stirred at 60 °C for 12 h, then the solid products were separated by a permanent magnet again and washed with deionized water.

2.4. Preparation of Fe_3O_4@ECS/PAA-Ag nanoparticles

50 mL dispersion of Fe_3O_4@ECS/PAA NPs was mixed with 40 mL of PVP aqueous solution (3.75×10^{-4} M). Then, 10 mL of freshly prepared aqueous solution of $[Ag(NH_3)_2]^+$ (0.15 M) was quickly added into the dispersion, stirred at room temperature for 1 h. Subsequently, this mixture was held at 70 °C and stirred for 7 h [36]. The final products were collected by a permanent magnet and washed with deionized water several times.

2.5. Characterizations

Transmission Electron Microscope (TEM) images were obtained with a Tecnal G2 20 S-Twin TEM at 200 kV. Fourier-Transform Infrared Spectra (FT-IR) were recorded on a Shimadzu IR Prestige-21 spectrometer with a diffuse reflectance attachment over a range from 500 to 4000 cm^{-1}. The X-Ray Diffraction (XRD) patterns of the samples were measured using a Bruker model D8 ADVANCE diffractometer with Cu Kα radiation (λ = 1.5418 nm). Thermal characterization of samples was carried out with the aid of Mettler Tory Thermogravimetric Analysis (TGA) operated at the heating rate of 20 °C/min under N_2. Magnetization curves as a function of magnetic field were measured at room temperature under magnetic field up to 10 kOe. The kinetics of silver ion release was monitored by PerkinElmer SCIEX ELAN DRCII Inductively Coupled Plasma Mass Spectrometry (ICP-MS).

2.6. Silver ion release study

The 10 mL Fe_3O_4@ECS/PAA-Ag nanoparticles (1 mg/mL) were added in a beaker containing 90 mL of PBS at 37 °C. At regular time intervals (4, 8, 12, 24, 36 and 48 h), 1 mL solution was taken and analyzed for the amount of Ag^+ by ICP-MS.

2.7. Antibacterial activity determination

Antibacterial testing was conducted against both *S. aureus* (ATCC 25923, Gram-positive) and Gram-negative *E. coli* (ATCC 25922). For the Inhibition Zone Test, a 0.1 mL of diluted bacterial suspension with 10^7–10^8 colony forming units per milliliter (CFU/mL) was taken to spread on the surface of the nutrient LB agar uniformly. Then three filter paper slices with the same size (1.5 cm) saturated with 40 μL of different nanoparticles (Fe_3O_4, Fe_3O_4@ECS/PAA, Fe_3O_4@ECS/PAA-Ag) dispersions (10 mg/mL) were placed onto the Petri dish and incubated at 37 °C for 24 h. For the kinetic test, 10 mg of antibacterial NPs were placed in a sterile bottle with 10 mL of bacteria suspension (10^7–10^8 CFU/mL) in PBS. After contact time of

30, 60, 90, 120, 150 min, respectively, the bottle was placed in a permanent separation stand for 2 min. Then, 100 μL of suspension was pipetted out, serially diluted to appropriate concentration, and spreaded on LB agar plates. Each dilution had three parallel groups. All the plates were incubated at 37 °C for 24 h and the numbers of the CFUs were inspected. Control experiment was conducted in the absence of samples.

Recyclable antibacterial activity of Fe_3O_4@ECS/PAA-Ag NPs was assessed by applying dynamic shaking flask method [23]. The as-prepared sample (20 mg) was incubated with 10 mL of cell suspension of both *E. coli* and *S. aureus* (10^6–10^7 CFU/mL) in 20 mL sterile bottle at 37 °C. After contact time of 120 min, the nanoparticles were recovered via magnetic force. The procedures described above were repeated, employing the same samples, ten more times.

3. Results and discussion

3.1. Preparation and characterizations of Fe_3O_4@ECS/PAA-Ag nanoparticles

The pathway applied to fabricate antibacterial nanostructures initially involved the formation of Fe_3O_4 NPs via chemical coprecipitation. Fig. 1a showed the FT-IR spectrum of Fe_3O_4 NPs. The strong absorption peak at around 540 cm^{-1} was characteristic of the Fe—O stretching vibration [9]. The corresponding TEM image was shown in Fig. 2a. The magnetic NPs were spherical or ellipsoidal with a distribution range (9–16 nm) and had a tendency to aggregate together. To prevent the aggregation and improve their dispersibility in aqueous solution, sodium citrate was used to modify the surface of Fe_3O_4 NPs. From Fig. 2b, obvious boundaries were observed between contacting nanoparticles.

Next, immobilization of CS coating onto Fe_3O_4 NPs was achieved with the aid of polymerization of acrylic acid. The synthetic method without crosslinking agent enhances utilization efficiency of CS [35]. Fig. 1b shows the FT-IR spectrum of Fe_3O_4@CS/PAA. The peak at 1720 cm^{-1} is ascribed to the stretching vibration of C═O bands from PAA. The characteristic absorption bands at 1570, 1375 and 1250 cm^{-1} are attributed to scissoring vibration of $-NH_2$, stretching vibration of —NHCO, and stretching vibration of C—O—C in CS polymeric backbone, respectively. The peak at 1030-1065 cm^{-1} is attributed to the combined effects of C—N stretching vibration of primary amines and the C—O stretching vibration from the primary alcohol. Then, Fe_3O_4@ECS/PAA nanoparticles were synthesized through modifying Fe_3O_4@CS/PAA with ethylenediamine. Fig. 1c shows the FTIR spectrum of Fe_3O_4@ECS/PAA. All characteristic peaks of CS became weakened, which revealed that the partial CS in polymeric coating was unstable and removed. However, the two peaks at 2860 and 2930 cm^{-1} corresponding to the symmetric and asymmetric stretching vibration of $-CH_2$ became stronger, confirming the successful ethylenediamine modification. Furthermore, the increasing intensity at 1030-1065 cm^{-1} indicated that ECS/PAA polymeric coating had more amine and hydroxyl groups than the unmodified coating [35]. The ECS/PAA copolymer layer would protect the magnetic core against oxidation, and provide the abundant hydrophilic groups.

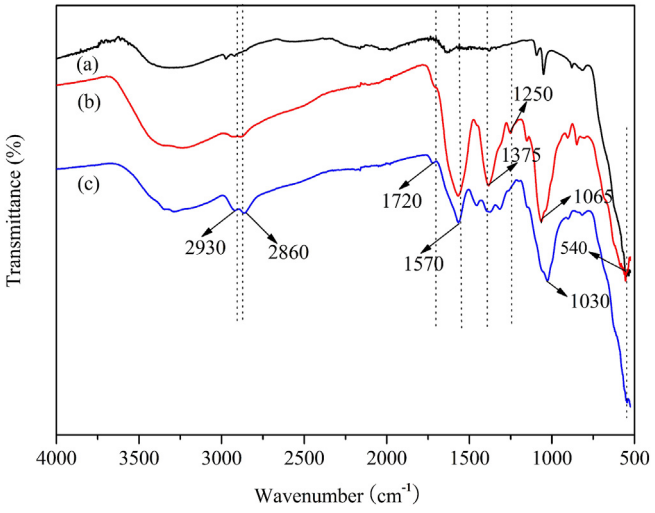

Fig. 1. FTIR spectra of (a) Fe_3O_4, (b) Fe_3O_4@CS/PAA and (c) Fe_3O_4@ECS/PAA.

The Ag NPs were deposited onto the magnetic nanoparticles by *in situ* reduction of $[Ag(NH_3)_2]^+$ with poly(vinyl pyrrolidone) as reductant and stabilizer in the presence of ECS/PAA polymer coating as template. The Fe_3O_4@ECS/PAA-Ag nanostructures were characterized by TEM as shown in Fig. 2c. The images exhibited that the well dispersed snowman-like heterodimers included an Ag NPs portion (black region) and a Fe_3O_4@ECS/PAA portion (gray region). The overall length of the heterodimers was around 45 nm, in which the mean diameter of Fe_3O_4@ECS/PAA NPs reached up to 35 nm, and that of Ag NPs was about 15 nm. The formation of heterodimeric nanostructures was probably the result of the nucleation and epitaxial growth of Ag nanocrystals on the ECS/PAA polymeric coatings of magnetite core [25].

Fig. 3 presents the XRD patterns of Fe_3O_4, Fe_3O_4@ECS/PAA and Fe_3O_4@ECS/PAA-Ag nanoparticles. The presence of diffraction peaks located at 2θ = 30.33°, 35.564°, 2.94°, 53.79°, 57.46°, and 63.18° in Fig. 3a coincide well with crystal indices of (220), (311), (400), (422), (511) and (440), respectively (JCPDS No. 65-3107), indicating the presence of a pure cubic phase of Fe_3O_4. In Fig. 3b and c, six peaks can again be indexed to the cubic phase of Fe_3O_4 core. Moreover, a broad peak appearing in the range from 13° to 33°is attributed to ECS/PAA polymer layer. In Fig. 3c, the diffraction peaks positioned at 2θ = 38.22°, 44.22°, 64.58°, and 77.57° correspond to (111), (220), (311), and (400) fcc crystal planes of pure silver, respectively, which also provides evidences for the deposition of Ag onto Fe_3O_4@ECS/PAA.

TGA measurements were performed for Fe_3O_4@ECS/PAA and Fe_3O_4@ECS/PAA-Ag nanocomposites. As shown in Fig. 4a, the Fe_3O_4@ECS/PAA NPs exhibited a two-stage weight loss process. The first weight loss of 1.66% until 120 °C was due to the evaporation of the physically adsorbed water or solvent. The second major weight loss of 41.34% from 120 to 515 °C was attributed to the decomposition of organic copolymer component in the shell layer of Fe_3O_4@ECS/PAA NPs. For the Fe_3O_4@ECS/PAA-Ag NPs (Fig. 4b), the weight loss of organic copolymer decomposition was 15.51%. According to the data above, the mass fraction of silver in the Fe_3O_4@ECS/PAA-Ag nanocomposites was estimated at about 63.1%. It could be proposed that ECS/PAA coating would facilitate deposition of Ag NPs on the surface of the Fe_3O_4 magnetic core.

Fig. 5 shows the magnetic hysteresis loops of Fe_3O_4 and Fe_3O_4@ECS/PAA-Ag NPs, which displayed superparamagnetic performance. The saturation magnetization value of Fe_3O_4@ECS/PAA-Ag NPs is 14.76 emu/g, which is much lower than that of the corresponding pristine Fe_3O_4 NPs (71.90 emu/g). But, this observed decrease in the saturation magnetization (79.47%) of Fe_3O_4@ECS/PAA-Ag agrees well with the mass decrement of Fe_3O_4 (78.62%) obtained from TGA measurements. Hence, the saturation magnetization possessed by unit mass of Fe3O4 nearly has no change. The formation of polymeric layer on Fe3O4 surface does not significantly affect the magnetic properties of the Fe_3O_4 NPs. Inset photograph in Fig. 5 shows that the Fe_3O_4@ECS/PAA-Ag nanostructures dispersed well in water and responded sharply to an

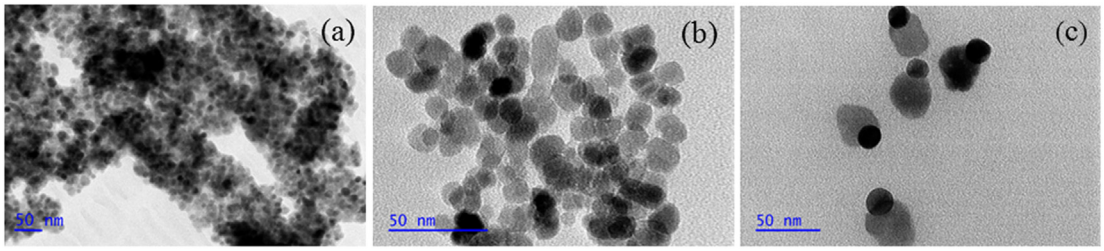

Fig. 2. TEM images of (a) Fe_3O_4, (b) Fe_3O_4 modified with sodium citrate and (c) Fe_3O_4@ECS/PAA-Ag.

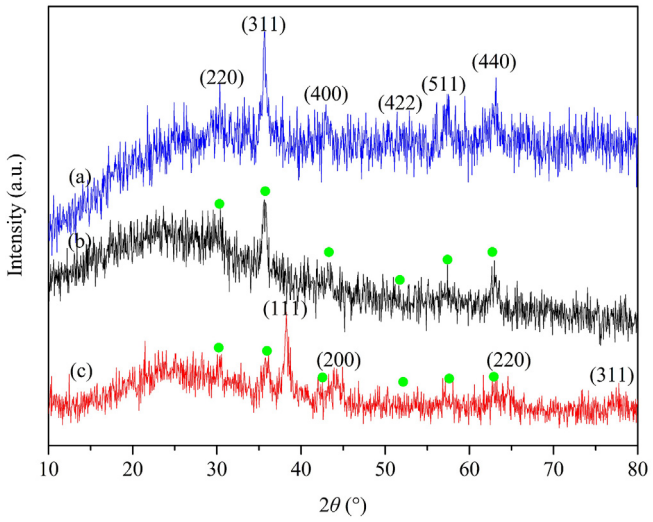

Fig. 3. XRD patterns of (a) Fe3O4, (b) Fe3O4@ECS/PAA and (c) Fe3O4@ECS/PAA-Ag. The reflections marked with a circular marker ( ) correspond to the cubic phase of Fe_3O_4 core.

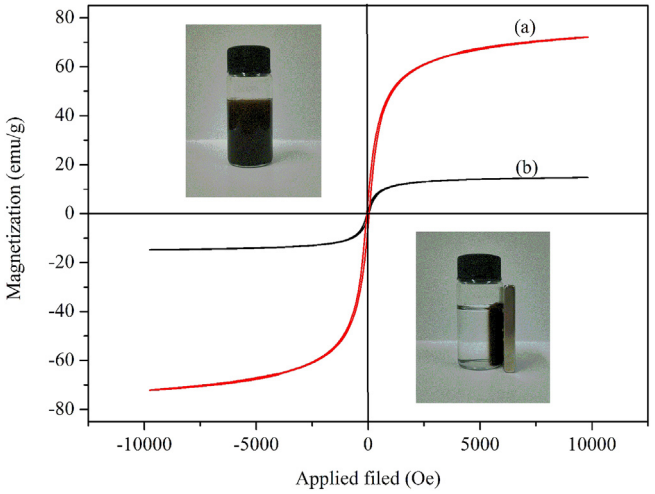

Fig. 5. Magnetization curves of (a) Fe_3O_4 and (b) Fe_3O_4@ECS/PAA-Ag.

external magnetic field. Therefore, it is expected that the nanocomposites can be easily recovered from the medium by the aid of an additional magnetic field.

The Ag^+ release behavior was determined and shown in Fig. 6. In general, the Ag + concentration dramatically increased in the first stage and then calmed down. The antibacterial performance of Fe_3O_4@ECS/PAA-Ag strongly depended on the Ag ions concentration released from the AgNPs [8].

3.2. Antibacterial activity

The antibacterial activity of as-prepared NPs was examined against Gram-positive bacteria *S. aureus* and Gram-negative bacteria *E. coli*. Fig. 7 displayed the optical images of the result of the inhibition zone test. There were clear zones of inhibition around the Fe_3O_4@ECS/PAA-Ag NPs, whereas no zone of inhibition was observed in the Fe_3O_4 and Fe_3O_4@ECS/PAA for both *E. coli* and *S. aureus* test. The formation of the obvious inhibition zone demonstrated that Fe_3O_4@ECS/PAA-Ag NPs could release silver ions

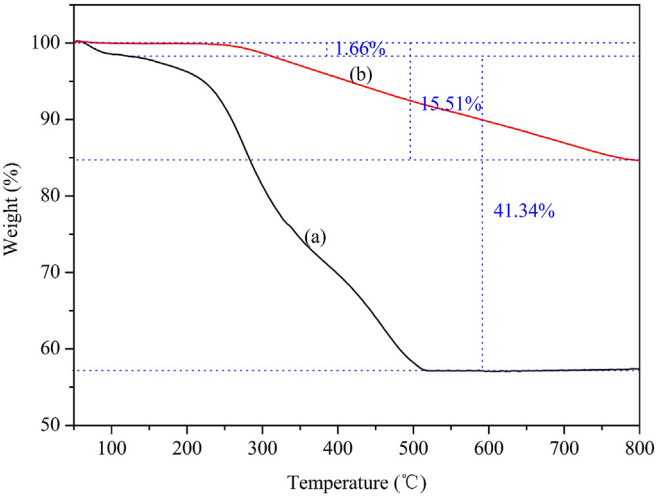

Fig. 4. TGA curves of (a) Fe_3O_4@ECS/PAA and (b) Fe_3O_4@ECS/PAA-Ag.

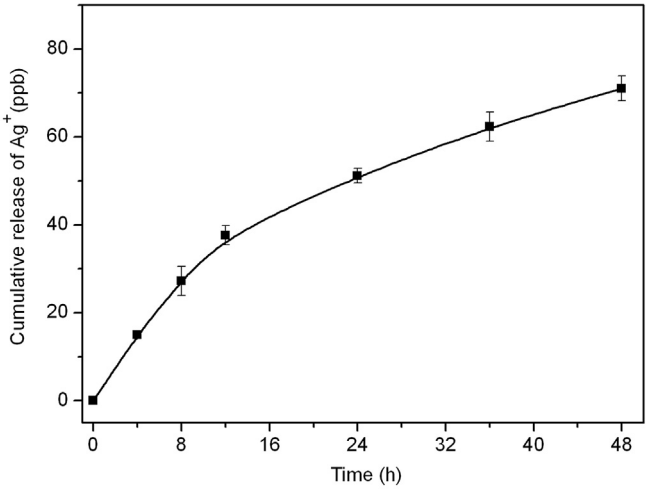

Fig. 6. Cumulative release profile of Ag^+ from Fe_3O_4@ECS/PAA-Ag.

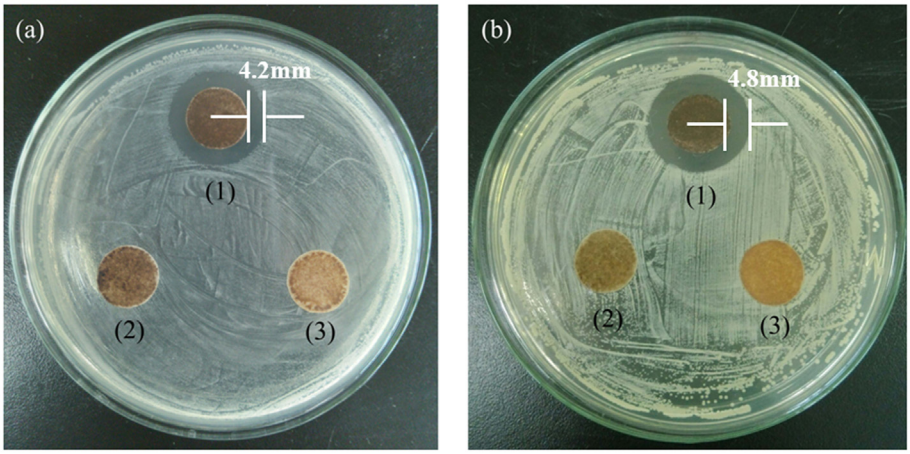

Fig. 7. Photographs of the zone of inhibition test against (a) *E. coli* and (b) *S. aureus* for (1) Fe_3O_4@ECS/PAA-Ag, (2) Fe_3O_4@ECS/PAA and (3) Fe_3O_4.

in the presence of water [8], which diffuse over time from nanoparticles surface, inducing the death of nearby bacteria.

The antibacterial properties of as-made samples were quantitatively assessed by a biocidal kinetic test shown in Fig. 8. The surviving cell of the control (without any samples) almost remained at 100% during 150 min, whereas Fe_3O_4@ECS/PAA NPs displayed obvious antibacterial activity for both *E. coli* and *S. aureus*. After 150 min exposure to the Fe_3O_4@ECS/PAA NPs, the residual live *E. coli* and *S. aureus* was 15.3% and 6.88%, respectively, which could be assigned to the antimicrobial action of modified CS/PAA coating. As we known, chitosan is a kind of "contact killing" antibacterial agents, which can adsorb free bacteria and induced the death of cells that contacted with them [30]. As no cytotoxic compounds were released out from antibacterial material, no zone of inhibition was observed around Fe_3O_4@ECS/PAA NPs. Furthermore, modified CS coated Fe_3O_4 NPs exhibited stronger bactericidal activity towards Gram-positive bacteria *S. aureus* than Gram-negative bacteria *E. coli*, which was consistent with general polycation compounds [28].

As shown in Fig. 8, Fe_3O_4@ECS/PAA-Ag NPs already inactivated 99.3% *E. coli* and 98.9% *S. aureus* in 30 min. After 60 min, as the contact time increased, the number of surviving bacterial colonies of *E. coli* was still dramatically reduced, while that of *S. aureus* had no significant change. After 150 min exposure to the Fe_3O_4@ECS/PAA-Ag NPs, the residual live *E. coli* and *S. aureus* were 0.003% and 0.103%, respectively. The results indicated that Fe_3O_4@ECS/PAA-Ag NPs possessed excellent antimicrobial activities for both two bacteria strains, which stemed from both Ag NPs and ECS/PAA polymeric coating. The dissolved silver released from Ag NPs contributed to the biocidal activity directly [8]. From the CFU reduction data for Fe_3O_4@ECS/PAA, the ECS/PAA coating itself displayed obvious antibacterial ability. Moreover, promoted by the electrostatic sorption of ECS/PAA coating to bacteria cell [30], Ag NPs of the heterodimeric nanostructures with a Zeta potential of +5.3 mV would adhere onto the bacteria surface and exert antibacterial function more effectively [37]. Contrary to Fe_3O_4@ECS/PAA, Fe_3O_4@ECS/PAA-Ag NPs displayed higher antibacterial efficiency toward Gram-negative *E. coli* than toward Gram-positive *S. aureus*. There was no doubt that the testing result was assigned to the antibacterial action of Ag NPs. Cell wall of Gram-positive bacteria have more peptidoglycan than that of Gram-negative bacteria. Since peptidoglycan includes abundant negatively charged groups, it can prevent Ag^+ from interacting with microorganism by combining with it. Therefore, Ag NPs exhibit more efficient toward Gram-negative bacteria than Gram-negative species [38].

Fig. 9 showed the antibacterial test data of the same magnetic nanoparticles through the whole ten exposure cycles. Between cycles, the magnetic nanoparticles were collected only by exposure to the external magnetic field without washing with water or any

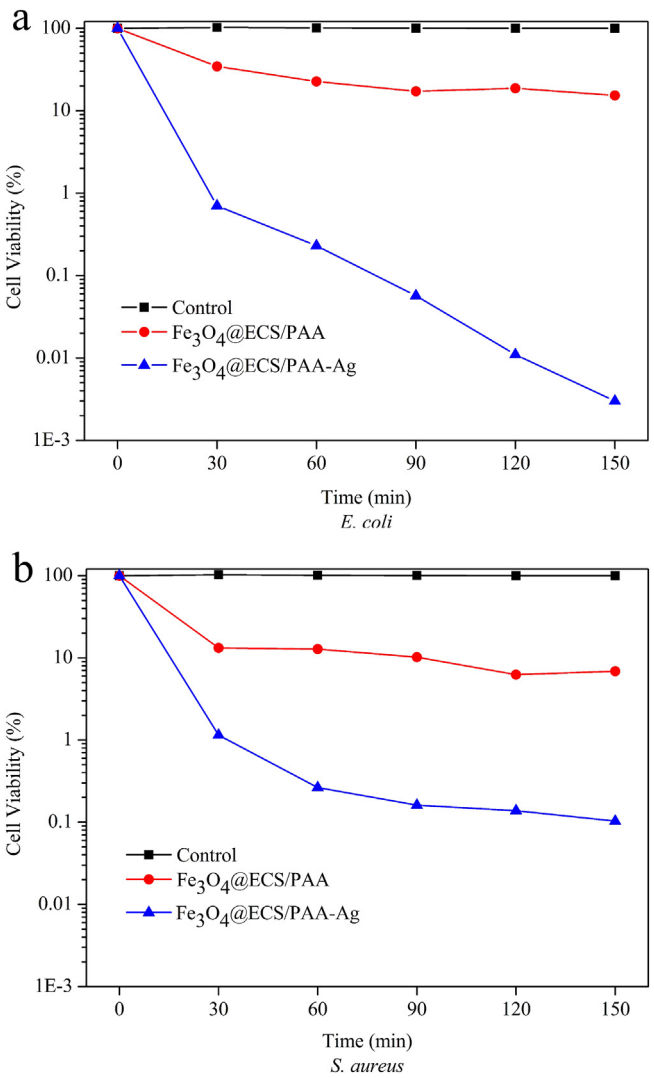

Fig. 8. Kinetics of antibacterial activity toward (a) *E. coli* and (b) *S. aureus* for Control, Fe_3O_4@ECS/PAA and Fe_3O_4@ECS/PAA-Ag.

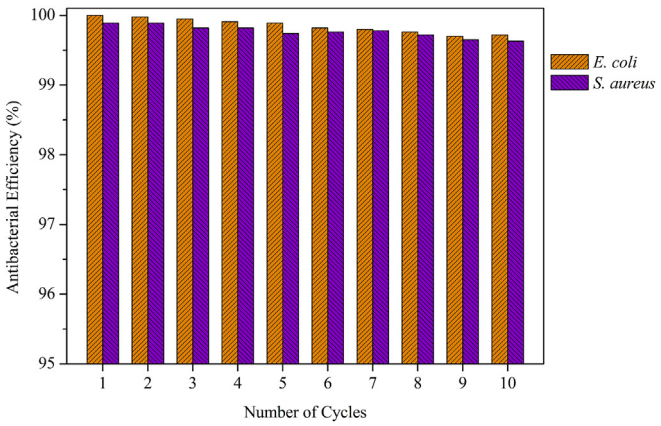

Fig. 9. Antibacterial activities of recycled Fe_3O_4@ECS/PAA-Ag against *E. coli* and *S. aureus*.

solvents. The bactericidal efficiency of Fe_3O_4@ECS/PAA-Ag NPs remained nearly 100% for both *E. coli* and *S. aureus*. Such considerably durable antibacterial efficiency may be mainly attributable to the high pure silver content of Fe_3O_4@ECS/PAA-Ag nanocomposites.

4. Conclusion

The antibacterial heterodimeric nanostructures of Fe_3O_4@ECS/PAA-Ag were successfully fabricated. The resultant nanocomposites composted of two distinct particles had a mean overall length of 45 nm and dispersed well in water. The mass fraction of silver in the as-made sample was at about 63.1%. In addition, considerably powerful and durable antibacterial performance of Fe_3O_4@ECS/PAA-Ag NPs was observed against both Gram-positive bacteria *S. aureus* and Gram-negative bacteria *E. coli*. In summary, the heterodimeric nanocomposites synthesized in this work realized the combination of dual antibacterial action and recyclable function, and could be a potential candidate for use in water purification, household sanitation, or even medical devices.

Acknowledgments

This research was supported by the funding from the National Natural Science Foundation of China (No. 81460107).

References

[1] S. Singh, D. Bahadur, Catalytic and antibacterial activity of Ag decorated magnetic core shell nanosphere, Colloids Surf.. B, Biointerfaces 133 (2015) 58–65.
[2] L.C. Wang, Y. Zhong, D. Widmann, J. Weissmüller, R.J. Behm, On the role of residual Ag in nanoporous Au catalysts for CO oxidation: a combined microreactor and TAP reactor study, ChemCatChem 4 (2) (2012) 251–259.
[3] P. Lee, J. Lee, H. Lee, J. Yeo, S. Hong, K.H. Nam, D. Lee, S.S. Lee, S.H. Ko, Highly stretchable and highly conductive metal electrode by very long metal nanowire percolation network, Adv. Mater. Deerf. Beach, Fla. 24 (25) (2012) 3326–3332.
[4] Siva Kumar-Krishnan, S. Chakaravarthy, A. Hernandez-Rangel, E. Prokhorov, G. Luna-Bárcenas, Rodrigo Esparza, M. Meyyappan, Chitosan supported silver nanowires as a platform for direct electrochemistry and highly sensitive electrochemical glucose biosensing, RSC Adv. 6 (24) (2016) 20102–20108.
[5] A.V. Yakovlev, O. Yu. Golubeva, Optimization of the synthesis and study of stable aqueous dispersions of silver nanoparticles used in medicine, Glass Phys. Chem. 39 (6) (2013) 643–648.
[6] V. Apalangyaa, V. Rangaria, B. Tiimoba, et al., Development of antimicrobial water filtration hybrid material from biosource calcium carbonate and silver nanoparticles, Appl. Surf. Sci. 295 (2014) 108–114.
[7] N.M. Huang, H.N. Lim, S. Radiman, P.S. Khiew, W.S. Chiu, R. Hashim, C.H. Chia, Sucrose ester micellar-mediated synthesis of Ag nanoparticles and the antibacterial properties, Colloids Surf. A Physicochem. Eng. Asp. 353 (1) (2010) 69–76.
[8] Z.M. Xiu, Q.B. Zhang, H.L. Puppala, V.L. Colvin, P.J. Alvarez, Negligible particle-specific antibacterial activity of silver nanoparticles, Nano Lett. 12 (8) (2012) 4271–4275.
[9] H.Q. Xia, B. Cui, J.H. Zhou, et al., Synthesis and characterization of Fe_3O_4@C@Ag nanocomposites and their antibacterial performance, Appl. Surf. Sci. 257 (2011) 9397–9402.
[10] Oliver Beier, Andreas Pfuch, Kerstin Horn, Jürgen Weisser, Matthias Schnabelrauch, Arnd Schimanski, Low temperature deposition of antibacterially active silicon oxide layers containing silver nanoparticles, prepared by atmospheric pressure Plasma chemical vapor deposition, Plasma Process. Polym. 10 (1) (2013) 77–87.
[11] M. Lismont, C.A. Páez, L. Dreesen, A one-step short-time synthesis of Ag@SiO_2 core-shell nanoparticles, J. Colloid Interface Sci. 447 (2015) 40–49.
[12] J.L. Song, N.L. Birbach, J.P. Hinestroza, Deposition of silver nanoparticles on cellulosic fibers via stabilization of carboxymethyl groups, Cellulose 19 (2012) 411–424.
[13] S.X. Hu, Y.L. Hsieh, Synthesis of surface bound silver nanoparticles on cellulose fibers using lignin as multi-functional agent, Carbohyd. Polym. 131 (2015) 134–141.
[14] R. Mohan, A.M. Shanmugharaj, R.S. Hun, An efficient growth of silver and copper nanoparticles on multiwalled carbon nanotube with enhanced antimicrobial activity, J. Biomed. Mater. Res. B 96 (2011) 119–126.
[15] X.L. Y, S. Li, J.H. Bao, et al., Immobilization of highly dispersed Ag nanoparticles on carbon nanotubes using electron-assisted reduction for antibacterial performance, ACS Appl. Mater. Interfaces 27 (2016) 17060–17067.
[16] C. Li, X. Wang, F. Chen, C. Zhang, X. Zhi, K. Wang, D. Cui, The antifungal activity of graphene oxide-silver nanocomposites, Biomaterials 34 (15) (2013) 3882–3890.
[17] A.F. de Faria, A.C.M. de Moraes, P.D. Marcato, et al., Eco-friendly decoration of graphene oxide with biogenic silver nanoparticles: antibacterial and antibiofilm activity, J. Nano. Res. 16 (2014) 1–16.
[18] Leila Shahriary, Roopa Nair, Sushma Sabharwal, Anjali A. Athawale, One-step synthesis of Ag–reduced graphene oxide–multiwalled carbon nanotubes for enhanced antibacterial activities, New J. Chem. 39 (6) (2015) 4583–4590.
[19] J.H. Yang, P. Zou, L.L. Yang, et al., A facile approach for the synthesis of magnetic separable Fe_3O_4@TiO_2, core-shell nanocomposites as highly recyclable photocatalysts, Appl. Surf. Sci. 288 (2014) 51–59.
[20] Q.H. Wu, C. Feng, C. Wang, et al., A facile one-pot solvothermal method to produce superparamagnetic graphene–Fe_3O_4 nanocomposite and its application in the removal of dye from aqueous solution, Colloids Surf. B Biointerfaces 101 (2013) 210–214.
[21] J.N. Gao, Y.J. He, X.Y. Zhao, et al., Single step synthesis of amine-functionalized mesoporous magnetite nanoparticles and their application for copper ions removal from aqueous solution, J. Colloid Interface Sci. 481 (2016) 220–228.
[22] B. Chudasama, A.K. Vala, N. Andhariya, et al., Enhanced antibacterial activity of bifunctional Fe_3O_4-Ag core-shell nanostructures, Nano. Res. 2 (2009) 955–965.
[23] Tamim Mosaiab, Chan Jin Jeong, Gyo Jic Shin, Kyung Ho Choi, Sang Kug Lee, Iksoo Lee, Insik In, Sung Young Park, Recyclable and stable silver deposited magnetic nanoparticles with poly (vinyl pyrrolidone)-catechol coated iron oxide for antimicrobial activity, Mater. Sci. Eng. C 33 (7) (2013) 3786–3794.
[24] H. Gu, Z. Yang, J. Gao, C.K. Chang, B. Xu, Heterodimers of nanoparticles: formation at a liquid-liquid interface and particle-specific surface modification by functional molecules, J. Am. Chem. Soc. 127 (1) (2005) 34–35.
[25] M. Lattuadaa, T.A. Hatton, Synthesis, properties and applications of Janus nanoparticles, Nano Today 6 (2011) 286–308.
[26] D.R. Kumar, D. Manoj, J. Santhanalakshmi, Au-ZnO bullet-like heterodimer nanoparticles: synthesis and use for enhanced nonenzymatic electrochemical determination of glucose, RSC Adv. 4 (2014) 8943–8952.
[27] Y. Mori, T. Ono, Y. Miyahira, et al., Antiviral activity of silver nanoparticle/chitosan composites against H1N1 influenza A virus, Nano, Res. Lett. 8 (2013) 1–6.
[28] A. Anitha, S. Sowmya, P.T.S. Kumar, et al., Chitin and chitosan in selected biomedical applications, Prog. Polym. Sci. 39 (2014) 1644–1667.
[29] João C. Fernandes, Freni K. Tavaria, José C. Soares, Óscar S. Ramos, M. João Monteiro, Manuela E. Pintado, F. Xavier Malcata, Antimicrobial effects of chitosans and chitooligosaccharides, upon Staphylococcus aureus and Escherichia coli, in food model systems, Food Microbiol. 25 (7) (2008) 922–928.
[30] Li Liu, Ling Xiao, Huayue Zhu, Xiaowen Shi, Preparation of magnetic and fluorescent bifunctional chitosan nanoparticles for optical determination of copper ion, Microchim. Acta 178 (3–4) (2012) 413–419.
[31] F. Kara, E.A. Aksoy, et al., Synthesis and surface modification of polyurethanes with chitosan for antibacterial properties, Carbohydr. Polym. 112 (2012) 39–47.
[32] J.H. Yang, P. Zou, L.L. Yang, et al., A comprehensive study on the synthesis and paramagnetic properties of PEG-coated Fe_3O_4 nanoparticles, Appl. Surf. Sci. 303 (2014) 425–432.
[33] X.H. Xue, J.H. Wang, L. Mei, et al., Recognition and enrichment specificity of Fe_3O_4 magnetic nanoparticles surface modified by chitosan and *Staphylococcus aureus* enterotoxins A antiserum, Colloids Surf. B Biointerfaces 103 (2013) 107–113.
[34] Y.H. Xu, Y. Zhou, W.H. Ma, et al., Highly sensitive and selective OFF-ON fluorescent sensor based on functionalized Fe_3O_4@SiO_2 nanoparticles for detection of Zn^{2+} in acetonitrile media, Appl. Surf. Sci. 276 (2013) 705–710.

[35] L.L. Zhou, Z.R. Liu, J.H. Liu, et al., Adsorption of Hg (II) from aqueous solution by ethylenediamine-modified magnetic crosslinking chitosan microspheres, Desalination 258 (2010) 41–47.
[36] Z. Deng, H. Zhu, B. Peng, H. Chen, Y. Sun, X. Gang, P. Jin, J. Wang, Synthesis of PS/Ag nanocomposite spheres with catalytic and antibacterial activities, ACS Appl. Mater. Interfaces 4 (10) (2012) 5625–5632.
[37] Alexander P. Richter, Joseph S. Brown, Bhuvnesh Bharti, Amy Wang, Sumit Gangwal, Keith Houck, Elaine A. Cohen Hubal, Vesselin N. Paunov, Simeon D. Stoyanov, Orlin D. Velev, An environmentally benign antimicrobial nanoparticle based on a silver-infused lignin core, Nat. Nanotechnol. 10 (9) (2015) 817–823.
[38] W.R. Li, X.B. Xie, Q.S. Shi, et al., Antibacterial effect of silver nanoparticles on *Staphylococcus aureus*, Biometals 24 (2011) 135–141.